Strengthening the case for interatomic Coulomb decay as a subdominant reaction channel in slow O^{3+}-Ne_2 collisions with independent-atom-model coupled-channel calculations

Dyuman Bhattacharya and Tom Kirchner*

Department of Physics and Astronomy, York University, Toronto, Ontario M3J 1P3, Canada

(Received 23 August 2020; accepted 19 November 2020; published 18 December 2020)

We report on electron removal calculations for 2.81 keV/amu Li^{3+} and O^{3+} ion collisions with neon dimers. The target is described as two independent neon atoms fixed at the dimer's equilibrium bond length, whose electrons are subjected to the time-dependent bare and screened Coulomb potentials of the classically moving Li^{3+} and O^{3+} projectile ions, respectively. Three mutually perpendicular orientations of the dimer with respect to the rectilinear projectile trajectories are considered and collision events for the two ion-atom subsystems are combined in an impact parameter by impact parameter fashion and are orientation averaged to calculate probabilities and cross sections for the ion-dimer system. The coupled-channel two-center basis generator method is used to solve the ion-atom collision problems. We concentrate the ion-dimer analysis on one-electron and two-electron removal processes which can be associated with interatomic Coulomb decay, Coulomb explosion, and radiative charge transfer. We find that the calculated relative yields are in fair agreement with recent experimental data for O^{3+}-Ne_2 collisions if we represent the projectile by a screened Coulomb potential, but disagree markedly for a bare Coulomb potential, i.e., for Li^{3+} impact. In particular, our calculations suggest that interatomic Coulomb decay is a significant reaction channel in the former case only, since capture of a Ne($2s$) electron to form hydrogenlike Li^{2+} is unlikely.

DOI: 10.1103/PhysRevA.102.062816

I. INTRODUCTION

Rare-gas dimers are much studied objects of the microworld with fascinating structural and dynamical properties. Their (van der Waals) bonds are weak and their internuclear distances large so that the two atoms appear to be (quasi-) independent. However, it has been demonstrated that charge and energy transfer between the two sites are possible and do happen after excitation by photon or charged-particle impact. Perhaps the most celebrated example of such a process is interatomic Coulomb decay (ICD), which is initiated by the removal of an inner-valence electron from one atom by the impinging particle or radiation. ICD then involves the transfer of the excitation energy to the other atom, its release in the form of (low-energy) outer-shell electron emission, and the fragmentation of the system of two singly charged ground-state ions produced in this way.

ICD was predicted in 1997 based on *ab initio* calculations [1]. The first experimental evidence was reported in a study of photoexcited neon clusters in 2003 [2] and was unequivocally confirmed for neon dimers one year later [3]. Since then, a large number of theoretical and experimental studies have provided further data and insight (see, e.g., Ref. [4] and references therein). ICD is now considered to be a ubiquitous process in a variety of systems, and the associated low-energy electron emission is deemed to play an important role in the radiation damage of biological tissue (see, e.g., Ref. [5] and references therein).

ICD in neon dimers subjected to slow multiply charged ion impact was reported in Ref. [6]. More specifically, kinetic energy release (KER) spectra for the $Ne^+(2p^{-1})$ + $Ne^+(2p^{-1})$ fragmentation channel (we use the same notation as the authors of Ref. [6] to indicate vacancies in a given atomic subshell) were recorded in coincidence with the final projectile charge state, and peaks in those spectra were associated with three different processes based on an analysis involving some of the potential energy curves of the dimer system. ICD resulting from the primary removal of one Ne($2s$) electron was one of these processes. The other two were radiative charge transfer (RCT) and Coulomb explosion (CE). The latter corresponds to the direct production of $Ne^+(2p^{-1})$ + $Ne^+(2p^{-1})$ in the collision by electron capture of one $2p$ electron from each atom, while the former is the result of a two-electron capture process from one atom, producing a transient state which relaxes radiatively to the same $Ne^+(2p^{-1})$ + $Ne^+(2p^{-1})$ channel as CE and ICD, but involves higher KER values. Relative yields for these processes were determined for three different projectile species: O^{3+}, Ar^{9+}, and Xe^{20+} ions. While RCT and CE were found to contribute for all three projectiles, the characteristic ICD peak was present only for O^{3+} impact, contributing 20% to the total yield.

These findings were supported by classical over-the-barrier model (COBM) calculations published along with the data. The calculations were based on an independent-atom-model (IAM) description of the ion-dimer collision problem using bare Coulomb potentials for the projectiles. For the O^{3+}-Ne_2 system they resulted in at most qualitative agreement with the measurements; in particular the ICD channel appeared to be too weak (contributing just 8.2% to the total yield),

*tomk@yorku.ca

while the CE yield was found to be significantly stronger than in the experiment. Given that the O^{3+}-Ne_2 system was the only one that showed evidence for ICD, an independent calculation based on a higher-level theory is desirable. This is the motivation for the present work.

Our calculations are also based on the IAM, but the ion-atom collisions are described in a semiclassical coupled-channel framework using the two-center basis generator method (TC-BGM) [7] to propagate the electronic wave function in the field of the classically moving nuclei. We combine electron removal probabilities in an impact parameter by impact parameter fashion for three perpendicular orientations of the dimer with respect to the rectilinear projectile trajectories and then orientation average the results to calculate absolute yields, i.e., cross sections, for the processes of interest. As it turns out, it is crucial to describe the O^{3+} ion by a screened Coulomb potential and take into account that its $2s$ subshell is occupied.

Our model is explained in Sec. II. In Sec. III we present and discuss our results in comparison with the experimental data and the previous COBM results. The paper ends with a few concluding remarks in Sec. IV. Atomic units, characterized by $\hbar = m_e = e = 4\pi\epsilon_0 = 1$, are used unless otherwise stated.

II. MODEL

The basic assumptions of our theoretical model are that (i) the projectile ion travels on a straight-line classical trajectory with constant speed v (semiclassical approximation), and (ii) the target system can be described as two independent atoms, fixed in space during the collision at a distance that corresponds to the equilibrium bond length R_e of the neon dimer. We use the value $R_e = 5.86$ a.u. [6,8]. Following the work of, e.g., Lühr and Saenz for collisions involving H_2^+ [9] and H_2 [10] we consider three perpendicular orientations of the target with respect to the projectile path: In orientation I, the dimer is aligned parallel to the projectile beam axis. In orientation II it is perpendicular to the projectile beam in the scattering plane, while in orientation III it is perpendicular to the scattering plane (see Fig. 1 of Ref. [9] for a sketch of the geometry). We calculate electronic transition probabilities for the processes of interest as functions of the (scalar) impact parameter b, measured with respect to the center of mass of the dimer, for these three orientations and construct an orientation average for each process j according to

$$P_j^{\rm ave}(b) = \tfrac{1}{3}\big[P_j^{\rm I}(b) + P_j^{\rm II}(b) + P_j^{\rm III}(b)\big]. \tag{1}$$

This orientation-averaged probability is then integrated over the impact parameter to calculate the cross section

$$\sigma_j^{\rm ave} = \int P_j^{\rm ave}(b)\, d^2b = 2\pi \int_0^\infty b P_j^{\rm ave}(b)\, db. \tag{2}$$

In the following subsection we describe how the ion-atom problem is solved. The subsequent Sec. II B deals with the combination of the ion-atom results to obtain probabilities and cross sections for the ion-dimer system.

A. Ion-atom collision calculations

The ion-atom collision calculations are carried out at the level of the independent electron model (IEM), i.e., electron-correlation effects are neglected and the Hamiltonian is assumed to have one-body character, $\hat{H}(t) \approx \sum_i \hat{h}_i(t)$, with a single-electron Hamiltonian of the form

$$\hat{h}(t) = -\tfrac{1}{2}\nabla^2 + v_T(r) + v_P(\mathbf{r}, t), \tag{3}$$

such that the many-electron time-dependent Schrödinger equation separates into a set of single-particle equations for the initially populated orbitals. In Eq. (3) v_T denotes a spherically symmetric effective target potential which includes the nuclear Coulomb potential (with charge number $Z_T = 10$ for Ne) and ground-state Hartree screening and exchange potentials obtained from the optimized potential method (OPM) of density functional theory (DFT) [11]. As a consequence of the exact treatment of exchange effects in the OPM, v_T falls off like $-1/r$ asymptotically and the exchange potential obtained from the numerical solution of the OPM integral equation exhibits a structure at intermediate r which can be interpreted as a manifestation of the shell structure of the atom [12].

The projectile potential v_P is a bare Coulomb potential with charge number $Z_P = 3$ for Li^{3+} projectiles and a screened Coulomb potential of Green-Sellin-Zachor [13] form for O^{3+}:

$$v_P(\mathbf{r}, t) = v_P(r_P) = -\frac{1}{r_P}\left[\frac{5}{1 + H(e^{r_P/d} - 1)} + 3\right]. \tag{4}$$

In Eq. (4) $r_P = |\mathbf{r} - \mathbf{R}(t)|$ is the distance between the active electron and the projectile nucleus, whose position vector follows the straight-line path $\mathbf{R}(t) = (\tilde{b}, 0, vt)$ where $\tilde{b}$ is the impact parameter with respect to the target atom [to be distinguished from the impact parameter b in Eqs. (1) and (2)]. The parameters $d = 0.476$ and $H = 3.02d$, taken from Table I of Ref. [14], were determined by a modified Hartree-Fock procedure described in that paper. The potential (4) interpolates between $-3/r_P$ for long and $-8/r_P$ for short distances, as it should from the perspective of an (active) electron placed on the target atom initially and ionized or captured by the projectile during the course of the collision. One can view our choice of Hamiltonian (3) as a no-response approximation to a full DFT treatment of the problem in which time-dependent electron-electron interaction effects are neglected [15,16].

The eight Ne L-shell electrons are propagated subject to the Hamiltonian (3) using a basis representation obtained from the TC-BGM, while the K-shell electrons are assumed to be passive. The K-shell electrons of the O^{3+} projectile ion are assumed to be passive as well, whereas the projectile L-shell electrons have to be treated with more care, as is explained further below.

The basis used includes the $2s$ to $4f$ target orbitals and all projectile orbitals from $1s$ ($2s$) to $7i$ for Li^{3+} (O^{3+}), augmented by electron-translation factors to ensure Galilean invariance. We use atomic orbitals with real instead of the standard complex spherical harmonics as their angular parts. This has the advantage that all basis states have even (*gerade*) or odd (*ungerade*) symmetry with respect to reflections about the scattering plane and do not mix during propagation. We denote these symmetry-adapted orbitals by the quantum numbers nlm_g and nlm_u in the following.

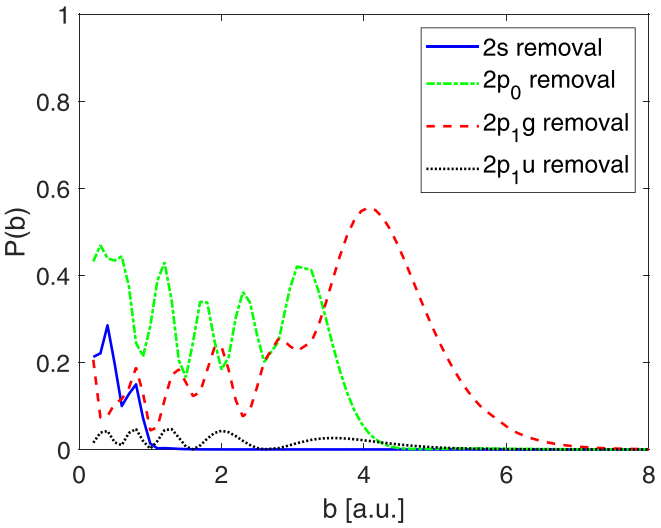

FIG. 1. Single-particle probabilities for electron removal from the Ne L shell by 2.81 keV/amu Li^{3+} impact plotted as functions of the impact parameter.

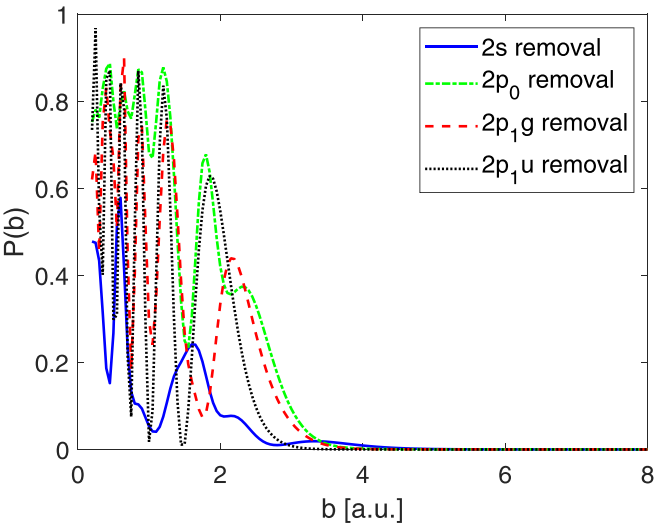

FIG. 2. Single-particle probabilities for electron removal from the Ne L shell by 2.81 keV/amu O^{3+} impact plotted as functions of the impact parameter. The probabilities are corrected for the presence of the projectile $2s$ electrons as described in the text.

The target and projectile two-center basis is further augmented by sets of 35 BGM pseudostates of gerade symmetry and 21 states of ungerade symmetry constructed in the usual way by operating with powers of a regularized projectile potential operator on the target eigenstates [7]. The asymptotic population of these states, when orthogonalized to the target and projectile two-center basis, can be interpreted as direct transfer to the continuum. Calculations have been carried out from an initial to a final projectile-target distance of 50 a.u. to ensure asymptotic convergence below the 1% level and on fine impact-parameter grids to resolve the rich structure at the impact energy of $E = 2.81$ keV/amu (corresponding to $v = 0.335$ a.u.), which was used in the experiment [6]. More details about the solution of the ion-atom collision problem using the TC-BGM are provided in Refs. [7,15].

Figure 1 shows the single-electron removal probabilities, obtained by exploiting the unitarity of the coupled-channel problem and subtracting the asymptotic target orbital populations from unity, for the Li^{3+} projectile. The probabilities are almost indistinguishable from the single-electron capture probabilities, i.e., direct transfer to the continuum is negligible (less than 0.5%). Clearly, electron removal is stronger for the initial Ne($2p_0$) and Ne($2p_{1g}$) electrons than for the $2s$ electrons which are more strongly bound and cannot be captured very efficiently into hydrogenlike Li^{2+}. Qualitatively, this can be understood by comparing the energy eigenvalues of the relevant target ($\varepsilon^{\rm OPM}_{{\rm Ne}(2s)} = -1.718$ a.u. versus $\varepsilon^{\rm OPM}_{{\rm Ne}(2p)} = -0.851$ a.u.) and projectile ($\varepsilon_{{\rm Li}^{2+}(n=2)} = -1.125$ a.u.) orbitals and keeping in mind that capture to lower-lying states is more likely because of the Stark shifts of the target states in the projectile potential. This simple argument suggests that capture of Ne($2p$) electrons to projectile states of principal quantum number $n = 2$ is the strongest channel, and indeed this is what the numerical calculations show. The removal of the Ne($2p_{1u}$) electrons is relatively weak, since fewer final states are available in the ungerade symmetry case. A more detailed analysis would require to compute correlation diagrams and quasimolecular couplings.

For O^{3+} impact the situation is complicated by the fact that Pauli blocking may prevent some electron capture transitions. As mentioned above, we consider both the Ne and the O^{3+} K-shell electrons as passive and do not include those states in the TC-BGM basis. This is justified by the large binding energies of the K-shell electrons and the weak couplings of the $1s$ states to other basis states. Such an approach does not work for the occupied L shells as some state-to-state couplings are strong and simply eliminating occupied states from the coupled-channel calculations contaminates some of the open channels. To illustrate these points, we note that in a TC-BGM calculation with the full basis the single-particle transfer probability from Ne($2s$) to $O^{3+}(2s)$ becomes very close to unity at some impact parameters, while test calculations in which the (occupied) $O^{3+}(2s)$ state was removed from the basis resulted in sizable transfer to the continuum—a process that should be ineffective at low collision energy.

In order to deal with this situation we subtracted the single-particle probabilities for the transitions Ne($2l$) $\rightarrow$ $O^{3+}(2s)$ from the Ne($2l$) electron removal probabilities and interpreted the results as the "true" removal probabilities. This seemingly naive procedure can be justified based on the principle of detailed balance [which asserts that the probability for a transition from, say, Ne($2s$) to $O^{3+}(2s)$ equals the probability for a transition from $O^{3+}(2s)$ to Ne($2s$)] and the inclusive probability formalism of Ref. [17]. The argument is presented in the Appendix.

We note that we ignored Pauli blocking due to the presence of one $2p$ electron in O^{3+} based on the rationale that this should be a weak effect given that five out of six states in the $2p$ subshell are vacant.

The resulting single-particle electron removal probabilities for O^{3+}-Ne collisions are presented in Fig. 2. Similarly to those of the Li^{3+}-Ne system (cf. Fig. 1) they show rich

structure as a function of impact parameter, but the details are quite different. Notably, all probabilities reach higher values, not far from unity for the Ne($2p$) initial states and up to 0.6 for Ne($2s$), the latter to be contrasted with a maximum removal probability $p_{2s}^{\rm rem}$ of approximately 0.3 for Li^{3+} impact. Also, $p_{2s}^{\rm rem}$ extends to significantly larger impact parameters for O^{3+} than for Li^{3+} projectiles, while the trend is opposite for $2p$ removal. The main reason for the increased probabilities in the $0 < b \lessapprox 2.5$ a.u. range is the lower energy eigenvalue of the (vacant) $O^{3+}(2p)$ orbitals at -1.868 a.u. as compared to -1.125 a.u. for hydrogenlike $Li^{2+}(2p)$, which makes capture (from all states) more effective. The increased Ne($2s$)-vacancy production probability will become important for the role of ICD to be discussed in the next section.

B. Analysis of electronic processes resulting in ICD, CE, and RCT

We now look at the neon dimer in each of the three orientations described above and combine ion-atom probabilities in an impact parameter by impact parameter fashion to calculate the probabilities on the right-hand side of Eq. (1) for the three processes of interest. For orientation I in which the dimer is parallel to the ion beam axis the situation is simple, since the impact parameters with respect to both atoms are the same and coincide with the impact parameter with respect to the center of mass of the dimer, i.e., $\tilde{b} \equiv b_{\rm I} = b$.

For each value of b considered, we proceed by determining the corresponding atomic impact parameters for orientations II and III and then carry out TC-BGM calculations at those impact parameters to avoid interpolations when combining and orientation averaging probabilities for the ion-dimer system. For orientation III in which the dimer is perpendicular to the scattering plane both atomic impact parameters are the same and are given by $b_{\rm III} = \sqrt{b^2 + (R_e/2)^2}$. For orientation II the two atomic impact parameters are different. The one with respect to the closer atom is $b_{\rm II}^{(1)} = |(R_e/2) - b|$ and the other one is $b_{\rm II}^{(2)} = b + (R_e/2)$.

As mentioned in the Introduction, ICD, CE, and RCT can be associated with specific one- and two-electron removal processes [6,18]. We calculate these processes by combining all products of single-particle probabilities which contribute to a given outcome, i.e., by a straightforward multinomial analysis of the combined ion–two-atom system. This approach corresponds to an IEM in which in addition to electron correlations the effects of the Pauli exclusion principle are neglected as well [16,19,20]. It has been used in a large number of theoretical studies of ion-atom and ion-molecule collision problems (see, e.g., Refs. [21–24] for recent examples).

Let us exemplify the procedure for the simplest case of orientation I in which both atomic impact parameters are the same. The probability for finding one vacancy in one of the Ne($2s$) orbitals is given by

$$P^{\rm I}_{2s^{-1}}(b) = 4p^{\rm rem}_{2s}(b_{\rm I})\big[1 - p^{\rm rem}_{2s}(b_{\rm I})\big]^3\big[1 - p^{\rm rem}_{2p_0}(b_{\rm I})\big]^4 \times \big[1 - p^{\rm rem}_{2p_{1g}}(b_{\rm I})\big]^4\big[1 - p^{\rm rem}_{2p_{1u}}(b_{\rm I})\big]^4, \tag{5}$$

where $b = b_{\rm I}$. The $(1 - p^{\rm rem}_{2s,2p})$ terms in this expression account for the requirement that all $2p$ electrons and three out of four $2s$ electrons of the two atoms remain bound. The multiplication factor of four arises because each of the four initial $2s$ electrons can be the one that is removed. The $2s$-vacancy process (5) can be associated with ICD.

Similarly, the probability for the removal of one $2p$ electron from each atom is given by

$$\begin{aligned} P^{\rm I}_{2p^{-1},2p^{-1}} = {} & \big(1 - p^{\rm rem}_{2s}\big)^4\big[2p^{\rm rem}_{2p_0}\big(1 - p^{\rm rem}_{2p_0}\big)\big(1 - p^{\rm rem}_{2p_{1g}}\big)^2 \\ & \times \big(1 - p^{\rm rem}_{2p_{1u}}\big)^2 + 2p^{\rm rem}_{2p_{1g}}\big(1 - p^{\rm rem}_{2p_{1g}}\big)\big(1 - p^{\rm rem}_{2p_0}\big)^2 \\ & \times \big(1 - p^{\rm rem}_{2p_{1u}}\big)^2 + 2p^{\rm rem}_{2p_{1u}}\big(1 - p^{\rm rem}_{2p_{1u}}\big)\big(1 - p^{\rm rem}_{2p_0}\big)^2 \\ & \times \big(1 - p^{\rm rem}_{2p_{1g}}\big)^2\big]^2, \end{aligned} \tag{6}$$

where we have omitted the impact parameter dependence for ease of notation. The first factor involving $p^{\rm rem}_{2s}$ ensures that no inner-valence vacancy is created. The three terms in square brackets account for the removal of one electron from either the $2p_0$, the $2p_{1g}$, or the $2p_{1u}$ orbital and the whole expression is squared to ensure that one-electron removal happens on both atoms simultaneously (and independently). The probability (6) can be associated with CE.

It was argued in Refs. [6,25] that double $2p$ removal from one atom may result in the third observed process, RCT, but not necessarily so, since the system can also dissociate as is, giving rise to one doubly charged and one neutral fragment. The experiment was blind to the latter channel and in the COBM calculations reported along with the measurements it was assumed that 50% of double removal from one atom will lead to RCT while the other 50% result in Ne^{2+} + Ne production [6].

Within the IEM, removing two $2p$ electrons from one atom while the other atom remains intact is represented by

$$\begin{aligned} P^{\rm I}_{2p^{-2}} = {} & 2\big(1 - p^{\rm rem}_{2s}\big)^4\big[\big(p^{\rm rem}_{2p_0}\big)^2\big(1 - p^{\rm rem}_{2p_{1g}}\big)^2\big(1 - p^{\rm rem}_{2p_{1u}}\big)^2 + \big(p^{\rm rem}_{2p_{1g}}\big)^2\big(1 - p^{\rm rem}_{2p_0}\big)^2\big(1 - p^{\rm rem}_{2p_{1u}}\big)^2 \\ & + \big(p^{\rm rem}_{2p_{1u}}\big)^2\big(1 - p^{\rm rem}_{2p_0}\big)^2\big(1 - p^{\rm rem}_{2p_{1g}}\big)^2 + 2p^{\rm rem}_{2p_0}\big(1 - p^{\rm rem}_{2p_0}\big)2p^{\rm rem}_{2p_{1g}}\big(1 - p^{\rm rem}_{2p_{1g}}\big)\big(1 - p^{\rm rem}_{2p_{1u}}\big)^2 \\ & + 2p^{\rm rem}_{2p_0}\big(1 - p^{\rm rem}_{2p_0}\big)2p^{\rm rem}_{2p_{1u}}\big(1 - p^{\rm rem}_{2p_{1u}}\big)\big(1 - p^{\rm rem}_{2p_{1g}}\big)^2 + 2p^{\rm rem}_{2p_{1g}}\big(1 - p^{\rm rem}_{2p_{1g}}\big)2p^{\rm rem}_{2p_{1u}}\big(1 - p^{\rm rem}_{2p_{1u}}\big)\big(1 - p^{\rm rem}_{2p_0}\big)^2\big] \\ & \times \big[\big(1 - p^{\rm rem}_{2p_0}\big)^2\big(1 - p^{\rm rem}_{2p_{1g}}\big)^2\big(1 - p^{\rm rem}_{2p_{1u}}\big)^2\big]. \end{aligned} \tag{7}$$

While this expression is lengthy, the interpretation of each term is straightforward. The first square bracket accounts for the removal of two electrons from one of the atoms from either the same $2p$ orbital or from two different orbitals, the latter terms being multiplied by two factors of two to account for the fact that both electrons in a given orbital are equally likely

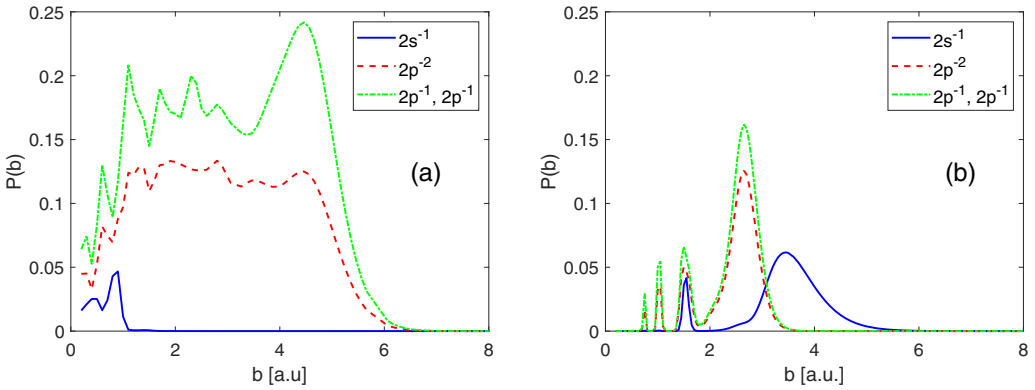

FIG. 3. Probabilities for $2s^{-1}$, $2p^{-2}$, and $(2p^{-1}, 2p^{-1})$ production in (a) Li^{3+} and (b) O^{3+} collisions with Ne_2 in orientation I at $E = 2.81$ keV/amu.

to be removed or not. The expression in the second square bracket takes care of the requirement that no $2p$ electron be removed from the second atom and the overall prefactor of two is there since it can be one or the other atom that is ionized. If one rearranges the terms in Eq. (7) and compares the whole expression with Eq. (6) one obtains

$$P^{\mathrm{I}}_{2p^{-1},2p^{-1}} - P^{\mathrm{I}}_{2p^{-2}} = 2\big(1-p^{\mathrm{rem}}_{2s}\big)^4\big(1-p^{\mathrm{rem}}_{2p_0}\big)^2\big(1-p^{\mathrm{rem}}_{2p_{1g}}\big)^2\big(1-p^{\mathrm{rem}}_{2p_{1u}}\big)^2\big[\big(p^{\mathrm{rem}}_{2p_0}\big)^2\big(1-p^{\mathrm{rem}}_{2p_{1g}}\big)^2\big(1-p^{\mathrm{rem}}_{2p_{1u}}\big)^2 + \big(p^{\mathrm{rem}}_{2p_{1g}}\big)^2\big(1-p^{\mathrm{rem}}_{2p_0}\big)^2\big(1-p^{\mathrm{rem}}_{2p_{1u}}\big)^2 + \big(p^{\mathrm{rem}}_{2p_{1u}}\big)^2\big(1-p^{\mathrm{rem}}_{2p_0}\big)^2\big(1-p^{\mathrm{rem}}_{2p_{1u}}\big)^2\big] \geqslant 0, \tag{8}$$

i.e., the prediction that CE is stronger than RCT, even if one makes the extreme assumption that double removal from one atom will always result in RCT.

This can be seen in Fig. 3 in which the probabilities (5) to (7) are plotted as functions of the impact parameter b for both Li^{3+} [Fig. 3(a)] and O^{3+} [Fig. 3(b)] collisions, using the same scales on the x and y axes to ease the comparison.

As can be expected from the ion-atom single-particle probabilities shown in Figs. 1 and 2 the results for the two projectiles are quite different. The $2p$ removal processes (6) and (7) are significantly stronger for Li^{3+} than for O^{3+} projectiles and extend to larger impact parameters. The first part of this observation may seem surprising given that the probabilities displayed in Fig. 1 (for Li^{3+}) tend to be smaller than those of Fig. 2 (for O^{3+}). However, one has to keep in mind that both Eqs. (6) and (7) include factors of the type $(1 - p^{\mathrm{rem}}_{2p})$ which correspond to the fact that 10 out of 12 $2p$ electrons are not removed. These factors act as effective suppression factors when the single-particle probabilities approach unity.

For the $2s$-vacancy production (5) the situation is reversed and the O^{3+} projectile is overall more effective than Li^{3+}. Again, it is a consequence of the $(1 - p^{\mathrm{rem}}_{2p})$ factors that the shallow maximum of the O^{3+}-impact $2s$ single-particle probability around $\tilde{b} \approx 3.3$ a.u. (cf. Fig. 2) results in the main peak of $P^{\mathrm{I}}_{2s^{-1}}$, while the process is mostly suppressed at smaller impact parameters.

For orientation III one can summarize the situation as follows: The expressions (5)–(7) remain unchanged except that the impact parameters on the left- and right-hand sides are now different, i.e., $b \neq b_{\mathrm{III}} = \sqrt{b^2 + (R_e/2)^2}$. One then sees (in Fig. 4) the probability distributions which occur at impact parameters $b \geqslant R_e/2$ in orientation I at smaller impact parameters and stretched out over a wider interval. The structures occurring at $b < R_e/2$ in orientation I are eliminated from the plot for orientation III, since the projectile never gets close enough to the two atoms. This is why the $2s$-vacancy production process is absent for Li^{3+} projectiles [Fig. 4(a)].

Orientation II in which the two atomic impact parameters are not the same, produces lengthier (but still straightforward) mathematical expressions and more complicated patterns for the three processes. This orientation does allow for $P_{2p^{-2}} > P_{2p^{-1},2p^{-1}}$ and in a quite pronounced way, in particular for O^{3+} projectiles as shown in Fig. 5(b). For this projectile the $P_{2p^{-1},2p^{-1}}$ probability is essentially zero except at $b < 1$ a.u., which can be understood by once again inspecting Fig. 2 and noticing that all $2p$ electron removal probabilities are small at atomic impact parameters larger than $R_e/2 = 2.93$ a.u. and are approaching zero rapidly toward more distant collisions. Given that both atoms need to be ionized for this process to occur and the farther atom in this orientation is at least a distance of $R_e/2$ away from the projectile, $P_{2p^{-1},2p^{-1}}$ is very small. By contrast, $P_{2p^{-2}}$ reaches substantial values, since both electrons can be efficiently removed from the closer atom. In this case, the obtained distribution is basically symmetric with respect to $b = R_e/2$ which corresponds to a head-on ion-atom collision. The same is true for the $2s$-vacancy production process, except that the shallow peak around $b \approx 6.4$ a.u. is too far out to have a mirror image at small impact parameters.

For Li^{3+} projectiles [Fig. 5(a)] the situation is different since the $2p$ single-particle removal probabilities extend beyond $b \approx R_e/2$ (cf. Fig. 1) and more substantial overlaps between contributions from the close and the far atom occur. The $2s$-vacancy production channel contributes in the interval $2 \lessapprox b \lessapprox 4$ a.u., as can be expected from Fig. 1 and Fig. 3(a):

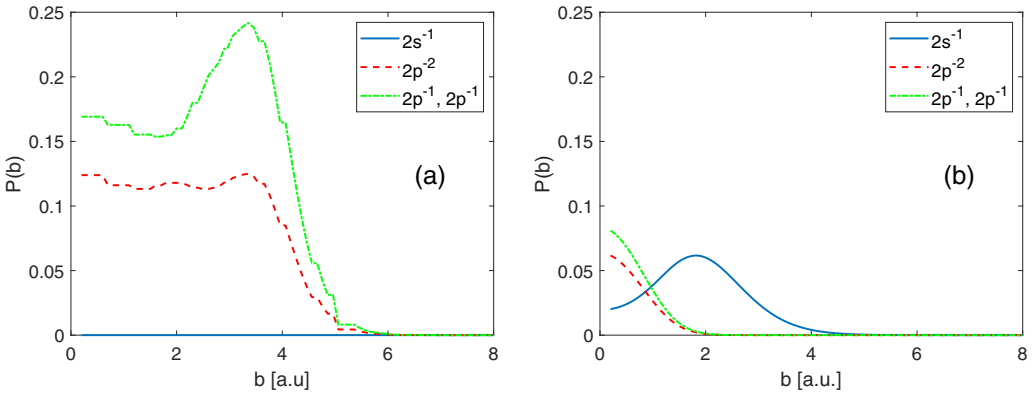

FIG. 4. Probabilities for $2s^{-1}$, $2p^{-2}$, and $(2p^{-1}, 2p^{-1})$ production in (a) Li^{3+} and (b) O^{3+} collisions with Ne_2 in orientation III at $E = 2.81$ keV/amu.

Only the closer atom can provide a nonzero p_{2s}^{rem} factor, and it does so only when the atomic impact parameter is one atomic unit or smaller. The distribution is not symmetric about $b = R_e/2$ because of the contributions from the $(1 - p_{2p}^{\text{rem}})$ factors from both atoms.

Figure 6 displays the orientation-averaged probabilities weighted by the impact parameter, i.e., the integrands of the cross-sectional formula (2) for the three processes of interest. The most obvious differences between the plots for both projectiles are that (i) both $2p$ removal processes are stronger for Li^{3+} [Fig. 6(a)] than for O^{3+} [Fig. 6(b)] and (ii) on a relative scale, the $2s$-vacancy production process and the process in which one $2p$ electron is removed from each atom switch roles: The former is by far the weakest channel for Li^{3+}, while the latter shows less area under the curve for O^{3+}, i.e., a smaller total cross section.

III. COMPARISON WITH EXPERIMENTAL AND COBM DATA AND DISCUSSION

We now discuss the relative yields obtained from comparing the total cross sections for the three processes. In order to compare the present results with the experimental data for ICD, CE, and RCT and the COBM calculations of Ref. [6] we apply the same correction as used in that work, namely we assume that only 50% of $P_{2p^{-2}}$ contributes to RCT, while 100% of $P_{2p^{-1},2p^{-1}}$ feeds into CE and 100% of $P_{2s^{-1}}$ into the ICD channel. The resulting relative yields (in percent) are shown in Table I. For our O^{3+} calculations we also show results obtained from the assumption that 100% of $P_{2p^{-2}}$ results in RCT.

Clearly, the calculations for O^{3+} projectiles are in better agreement with the measurements than those for Li^{3+} impact. In particular, they give the experimentally observed ordering CE < ICD < RCT, while both the Li^{3+} TC-BGM and the COBM calculation of Ref. [6] appear to overemphasize the CE channel and underestimate ICD. These two calculations make different predictions about which one is the strongest channel, but are nevertheless in fair agreement with each other.

The fact that the present results for O^{3+} are in almost perfect agreement with the experimental yields when the "100% assumption" is applied to the $2p^{-2}$ channel should perhaps not be overinterpreted given that our model has several limitations: First, reinspecting Figs. 3 to 5 one observes that the orientation dependence is quite strong. This raises the question whether an orientation average involving more than three orientations might yield a different result. While ultimately this can be answered only by additional calculations we note that in their work for collisions involving H_2^+ [9] and H_2 [10] Lühr and Saenz also found considerable orientation dependence but concluded that averages

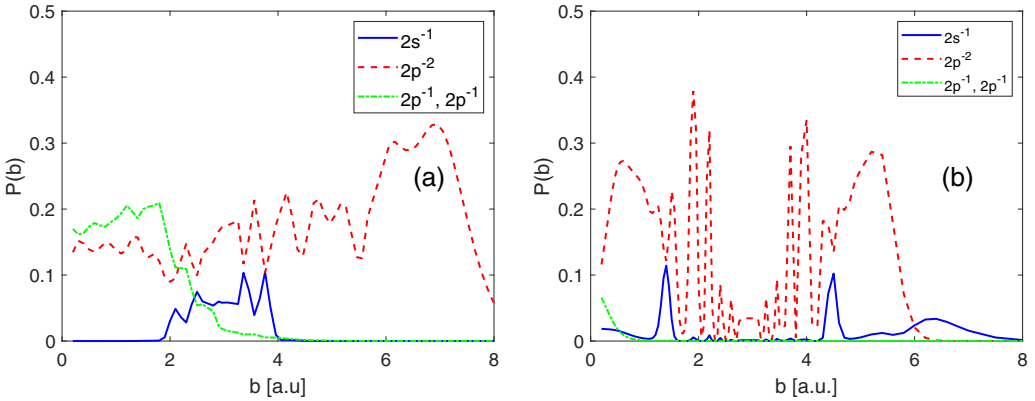

FIG. 5. Probabilities for $2s^{-1}$, $2p^{-2}$, and $(2p^{-1}, 2p^{-1})$ production in (a) Li^{3+} and (b) O^{3+} collisions with Ne_2 in orientation II at $E = 2.81$ keV/amu.

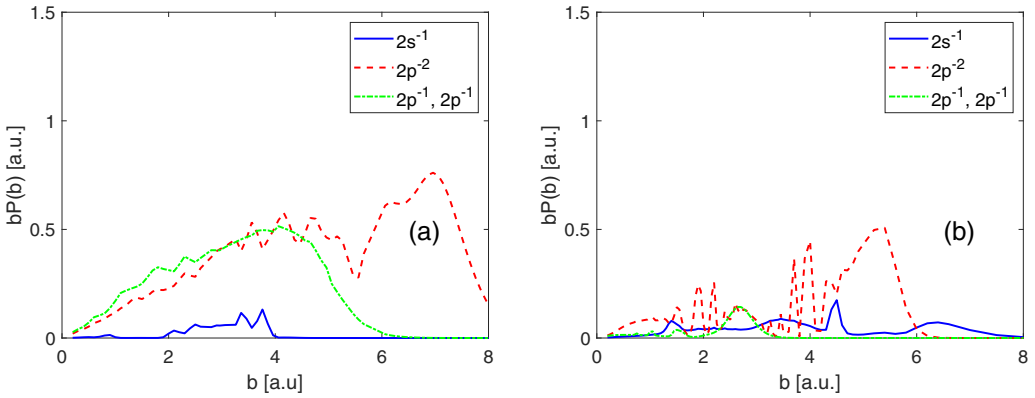

FIG. 6. Orientation-averaged impact-parameter-weighted probabilities for $2s^{-1}$, $2p^{-2}$, and $(2p^{-1}, 2p^{-1})$ production in (a) Li^{3+} and (b) O^{3+} collisions with Ne_2 at $E = 2.81$ keV/amu.

based on the three perpendicular orientations only were rather accurate.

Second, the IAM for the dimer coupled with the IEM for the electrons of both atoms provides of course only an approximate framework for the discussion of the collision problem at hand. In recent work for a large variety of multicenter systems, ranging from small covalent molecules to large clusters and biomolecules, an amended IAM was explored, in which the geometric overlap of effective atomic cross sectional areas was taken into account [15,26,27]. However, that model has so far been applied only to net cross sections and not to the more detailed one- and two-electron removal processes studied here. While such an extension is outstanding, one can perhaps argue that overall geometric overlap should be small for a system such as Ne_2 whose internuclear distance is large, but that it would affect the three orientations considered differently and would amount to their reweighting in the calculation of the orientation average. To estimate the potential effect we applied the extreme assumption that the orientation I probabilities are to be divided by a factor of two to account for the complete overlap of the atomic cross sectional areas when viewed from the position of the impinging projectile, while the results for the other two orientations remain unchanged. We found that the relative yields do change, but not very dramatically. In particular, the ICD yields decrease from 34.7% and 22.7% for the two models shown in Table I to 34.0% and 21.6%.

It is more difficult to estimate the error associated with using the IEM, or, in other words, the effects of electron correlations, which we have neglected in order to simplify the treatment. While it is known that they do play a role in collisional multielectron dynamics [19,28,29], it is not clear how they affect the relative yields of interest here. First-principles many-electron calculations would be required to shed light on this issue. In their absence, we can say only that the fair agreement between our O^{3+} results and the experimental data does not suggest that electron correlations are of major importance.

IV. CONCLUDING REMARKS

Motivated by a recent joint experimental and theoretical work [6], we have studied specific one- and two-electron removal processes in Li^{3+} and O^{3+} collisions with neon dimers at $E = 2.81$ keV/amu, representing the target system as two independent atoms and accounting for the ion-atom electron dynamics at the level of the independent electron model. The coupled-channel two-center basis generator method has been used to solve the single-particle Schrödinger equation for all active target electrons taking into account in the O^{3+} case that the projectile potential is of screened Coulomb character and that the $2s$ subshell is occupied.

We find that the results for both projectiles are markedly different and only the O^{3+} calculations yield fair agreement with experimental data for ICD, CE, and RCT. In particular, our calculations suggest that ICD is so weak a process for bare projectiles that it might be hard to measure it. This is a new piece of information given that the classical calculation of Ref. [6] predicted a somewhat higher ICD yield for Li^{3+} impact.

Together with the conclusion of that paper that ICD can be observed only in lowly charged ion collisions (because $2s$ removal is overwhelmed by additional $2p$ removal for more

TABLE I. Relative yields (in percent) for the three processes of interest. The TC-BGM results marked with a star are obtained from the assumption that 100% of $P_{2p^{-2}}$ contributes to RCT, while in the other columns it is assumed that only 50% contributes to this channel. The COBM and experimental data are from Ref. [6].

	COBM (Li^{3+})	TC-BGM (Li^{3+})	TC-BGM (O^{3+})	TC-BGM (O^{3+})*	Expt.
$2s^{-1}$ (ICD)	8.0	3.6	34.7	22.7	20
$2p^{-1}, 2p^{-1}$ (CE)	39.3	50.2	12.5	8.2	10
$2p^{-2}$ (RCT)	52.7	46.2	52.8	69.1	70

highly charged projectiles) one may say that a fine balance of charge state and structure of a projectile is required to make ICD a significant process in low-energy capture collisions. It would be interesting to see if this can be confirmed by COBM calculations with effective projectile potentials like the one used in this work [Eq. (4)] and if one can identify an optimal projectile that maximizes the ICD yield. Future work should also be concerned with a more systematic study of the relative strengths of ICD, CE, and RCT over a range of projectile species and energies and also for different target systems, such as water clusters. A more quantitative understanding of the ICD process in particular may have important implications for ion-beam cancer therapy, since the low-energy electrons it produces are effective agents for inflicting cellular damage.

ACKNOWLEDGMENTS

Financial support from the Natural Sciences and Engineering Research Council of Canada (NSERC) (RGPIN-2019-06305) is gratefully acknowledged. We thank Amine Cassimi for providing us with the experimental and COBM yields listed in Table I.

APPENDIX

Let us consider a simplified problem with just two spin-parallel electrons occupying the target and projectile $2s$ states $|2s^T\rangle$ and $|2s^P\rangle$ before the collision. We denote the solutions of the single-particle equations for both electrons at a final time t_f after the collision by $|\psi_{2s^T}\rangle$ and $|\psi_{2s^P}\rangle$. Within the IEM the two-electron problem is represented by a Slater determinant composed of these two single-particle states.

As shown in Ref. [17], when using determinantal wave functions the inclusive probability for finding one electron in $|2s^T\rangle$ after the collision while the other one is not observed is given by the one-particle density matrix element

$$\langle 2s^T|\hat{\gamma}|2s^T\rangle = |\langle 2s^T|\psi_{2s^T}\rangle|^2 + |\langle 2s^T|\psi_{2s^P}\rangle|^2. \tag{A1}$$

Not observing one electron implies that it can be anywhere but in the $2s$ target state, which is blocked by the other electron. Hence, we can interpret

$$P^T_{\rm vac} \equiv 1 - \langle 2s^T|\hat{\gamma}|2s^T\rangle \tag{A2}$$

as the probability for finding the $2s$ target state vacant after the collision. The principle of detailed balance demands that $|\langle 2s^T|\psi_{2s^P}\rangle|^2 = |\langle 2s^P|\psi_{2s^T}\rangle|^2$, provided both electrons are propagated in the same single-particle Hamiltonian. We have checked that our TC-BGM solutions are consistent with this result. Accordingly, we can write

$$P^T_{\rm vac} = 1 - |\langle 2s^T|\psi_{2s^T}\rangle|^2 - |\langle 2s^P|\psi_{2s^T}\rangle|^2, \tag{A3}$$

i.e., the $2s$ target vacancy probability is obtained by subtracting the $2s^T \to 2s^P$ transition probability from the probability that the initial target electron is not found in its initial $2s$ state. Given that target excitation is a weak process in the collision system studied in this work, we can interpret the latter as the target electron removal probability.

The same argument applies to the initial $2p$ target electrons and can readily be extended to several target electrons and both spin directions (given that spin flips are impossible for a spin-independent Hamiltonian). This justifies our (approximate) procedure to determine the "true" single-particle removal probabilities by subtracting the probabilities for $\mathrm{Ne}(2l) \to \mathrm{O}^{3+}(2s)$ from the original $\mathrm{Ne}(2l)$ electron removal probabilities.

[1] L. S. Cederbaum, J. Zobeley, and F. Tarantelli, Phys. Rev. Lett. **79**, 4778 (1997).
[2] S. Marburger, O. Kugeler, U. Hergenhahn, and T. Möller, Phys. Rev. Lett. **90**, 203401 (2003).
[3] T. Jahnke, A. Czasch, M. S. Schöffler, S. Schössler, A. Knapp, M. Käsz, J. Titze, C. Wimmer, K. Kreidi, R. E. Grisenti *et al.*, Phys. Rev. Lett. **93**, 163401 (2004).
[4] T. Jahnke, J. Phys. B: At. Mol. Opt. Phys. **48**, 082001 (2015).
[5] X. Ren, E. Wang, A. D. Skitnevskaya, A. B. Trofimov, K. Gokhberg, and A. Dorn, Nat. Phys. **14**, 1062 (2018).
[6] W. Iskandar, J. Matsumoto, A. Leredde, X. Fléchard, B. Gervais, S. Guillous, D. Hennecart, A. Méry, J. Rangama, C. L. Zhou *et al.*, Phys. Rev. Lett. **114**, 033201 (2015).
[7] M. Zapukhlyak, T. Kirchner, H. J. Lüdde, S. Knoop, R. Morgenstern, and R. Hoekstra, J. Phys. B **38**, 2353 (2005).
[8] S. M. Cybulski and R. R. Toczyłowski, J. Chem. Phys. **111**, 10520 (1999).
[9] A. Lühr and A. Saenz, Phys. Rev. A **80**, 022705 (2009).
[10] A. Lühr and A. Saenz, Phys. Rev. A **81**, 010701(R) (2010).
[11] E. Engel and S. H. Vosko, Phys. Rev. A **47**, 2800 (1993).
[12] E. Engel and R. M. Dreizler, J. Comput. Chem. **20**, 31 (1999).
[13] A. E. S. Green, D. L. Sellin, and A. S. Zachor, Phys. Rev. **184**, 1 (1969).
[14] P. P. Szydlik and A. E. S. Green, Phys. Rev. A **9**, 1885 (1974).
[15] H. J. Lüdde, M. Horbatsch, and T. Kirchner, Eur. Phys. J. B **91**, 99 (2018).
[16] T. Kirchner, L. Gulyás, H. J. Lüdde, E. Engel, and R. M. Dreizler, Phys. Rev. A **58**, 2063 (1998).
[17] H. J. Lüdde and R. M. Dreizler, J. Phys. B **18**, 107 (1985).
[18] A. Cassimi, X. Fléchard, B. Gervais, A. Méry, and J. Rangama, in *Ion-Atom Collisions: The Few-Body Problem in Dynamic Systems*, edited by M. Schulz (De Gruyter, Berlin, 2019), p. 213.
[19] J. H. McGuire, *Electron Correlation Dynamics in Atomic Collisions* (Cambridge University Press, Cambridge, 1997).
[20] M. M. Sant'Anna, E. C. Montenegro, and J. H. McGuire, Phys. Rev. A **58**, 2148 (1998).
[21] C. C. Montanari and J. E. Miraglia, J. Phys. B **45**, 105201 (2012).

[22] T. Kirchner, N. Khazai, and L. Gulyás, Phys. Rev. A **89**, 062702 (2014).
[23] A. C. K. Leung and T. Kirchner, Phys. Rev. A **95**, 042703 (2017).
[24] P. N. Terekhin, M. A. Quinto, J. M. Monti, O. A. Fojón, and R. D. Rivarola, J. Phys. B **51**, 235201 (2018).
[25] W. Iskandar, X. Fléchard, J. Matsumoto, A. Leredde, S. Guillous, D. Hennecart, J. Rangama, A. Méry, B. Gervais, H. Shiromaru, and A. Cassimi, Phys. Rev. A **98**, 012701 (2018).
[26] H. J. Lüdde, A. Achenbach, T. Kalkbrenner, H.-C. Jankowiak, and T. Kirchner, Eur. Phys. J. D **70**, 82 (2016).
[27] H. J. Lüdde, T. Kalkbrenner, M. Horbatsch, and T. Kirchner, Phys. Rev. A **101**, 062709 (2020).
[28] D. Belkić, I. Mančev, and J. Hanssen, Rev. Mod. Phys. **80**, 249 (2008).
[29] F. Aumayr, K. Ueda, E. Sokell, S. Schippers, H. Sadeghpour, F. Merkt, T. F. Gallagher, F. B. Dunning, P. Scheier, O. Echt *et al.*, J. Phys. B: At. Mol. Opt. Phys. **52**, 171003 (2019).